Biochimica et Biophysica Acta 1808 (2011) 2214–2223

Contents lists available at ScienceDirect

Biochimica et Biophysica Acta

journal homepage: www.elsevier.com/locate/bbamem

A minimal isoform of the TMEM16A protein associated with chloride channel activity

Loretta Ferrera, Paolo Scudieri, Elvira Sondo, Antonella Caputo [1], Emanuela Caci, Olga Zegarra-Moran, Roberto Ravazzolo, Luis J.V. Galietta *

Laboratorio di Genetica Molecolare, Largo Gerolamo Gaslini, Istituto Giannina Gaslini, 16147 Genova, Italy

ARTICLE INFO

Article history:
Received 11 February 2011
Received in revised form 11 April 2011
Accepted 20 May 2011
Available online 30 May 2011

Keywords:
Chloride channel
Alternative splicing
Intracellular calcium
Patch-clamp

ABSTRACT

TMEM16A protein, also known as anoctamin-1, has been recently identified as an essential component of Ca^{2+}-activated Cl^- channels. We previously reported the existence of different TMEM16A isoforms generated by alternative splicing. In the present study, we have determined the functional properties of a minimal TMEM16A protein. This isoform, called TMEM16A(*0*), has a significantly shortened amino-terminus and lacks three alternative segments localized in the intracellular regions of the protein (total length: 840 amino acids). TMEM16A(*0*) expression is associated with Ca^{2+}-activated Cl^- channel activity as measured by three different functional assays based on the halide-sensitive yellow fluorescent protein, short-circuit current recordings, and patch-clamp technique. However, compared to a longer isoform, TMEM16(*abc*) (total length: 982 amino acids), TMEM16A(*0*) completely lacks voltage-dependent activation. Furthermore, TMEM16A(*0*) and TMEM16A(*abc*) have similar but not identical responses to extracellular anion replacement, thus suggesting a difference in ion selectivity and conductance. Our results indicate that TMEM16A(*0*) has the basic domains required for anion transport and Ca^{2+}-sensitivity. However, the absence of alternative segments, which are present in more complex isoforms of TMEM16A, modifies the channel gating and ion transport ability.

1. Introduction

Ca^{2+}-activated Cl^- channels (CaCCs) have important physiological roles in many cell types and tissues such as the surface epithelium of the airways, the secretory cells of exocrine glands, olfactory cells, and the smooth muscle of blood vessels, bronchi, and gastrointestinal apparatus [1]. The biophysical properties, pharmacological sensitivity, and regulation of CaCCs are in part cell type-dependent thus suggesting a heterogeneity of the CaCC components. For example, some CaCCs are activated by depolarization [2–7] whereas others are voltage-independent [8–10]. Recently, the TMEM16A protein (also named anoctamin-1) was found to be associated with CaCC activity [11–13]. Indeed, silencing of endogenous TMEM16A expression causes inhibition of Ca^{2+}-dependent Cl^- transport. Furthermore, overexpression of TMEM16A in null cells evokes the appearance of voltage- and Ca^{2+}-activated Cl^- currents. Finally, selective mutagenesis of conserved residues in the TMEM16A protein sequence alters the properties of the resulting Cl^- currents [11,13]. These results constitute evidence that the TMEM16A protein is an essential component of CaCCs. TMEM16B (anoctamin-2), a close paralog of TMEM16A, is also associated with Ca^{2+}-dependent Cl^- channel activity [12,14–16]. The more distant paralogs of TMEM16A protein [17] may be associated with non-channel function. For example, TMEM16F has been recently found to work as a Ca^{2+}-dependent phosphatidylserine scramblase [18].

In previous studies, we have shown the existence of multiple TMEM16A isoforms which are characterized by inclusion/skipping of four segments labeled as *a* (116 residues), *b* (22 residues), *c* (4 residues), and *d* (26 residues) [11,19]. The segment *a*, which is localized at the N-terminus, can be skipped when an alternative promoter is used. The presence of segments *b*, *c*, and *d*, is instead controlled by alternative splicing of exons 6b, 13, and 15, respectively. Most abundant TMEM16A isoforms are (*ac*), (*abc*), and (*acd*). However, we also found evidence of a protein lacking all alternative segments and therefore called TMEM16A (*0*) [11]. Although rare, this minimal version of the TMEM16A protein is interesting to identify the protein domains involved in channel function. In the present study, we have determined the functional characteristics of TMEM16A(*0*). Our results show that this isoform is indeed active, associated with anion transport, and activated by Ca^{2+}. However, the lack of alternative segments alters various channel properties such as voltage-dependence and ion selectivity.

2. Materials and methods

2.1. Cell culture

Fischer rat thyroid (FRT) cells were cultured in Coon's modified Ham's F-12 medium. HEK-293 cells were instead cultured in DMEM/Ham's F12

Abbreviations: CaCC, Ca^{2+}-activated Cl^- channel; YFP, yellow fluorescent protein

* Corresponding author. Tel.: +39 10 5636801; fax: +39 10 3779797.
E-mail address: galietta@unige.it (L.J.V. Galietta).
[1] Present address: Dip. Psichiatria e Neurobiologia, Universita` di Pisa, via Bonanno 6, 56126 Pisa, Italy.

0005-2736 © 2011 Elsevier B.V. Open access under CC BY-NC-ND license.
doi:10.1016/j.bbamem.2011.05.017

(1:1). Both media were supplemented with 10% fetal calf serum, 2 mM L-glutamine, 100 U/ml penicillin, and 100 μg/ml streptomycin.

2.2. Transient transfections

For the YFP-based functional assay, HEK-293 cells were seeded in 96-well microplates (25,000 cells/well) in 100 μl of antibiotic-free culture medium. After 6 hours, cells were co-transfected with plasmids carrying the coding sequence for TMEM16A isoforms and the halide sensitive yellow fluorescent protein YFP-H148Q/I152L [20]. For each well, 0.2 μg of total plasmid DNA and 0.5 μl of Lipofectamine 2000 (Invitrogen) were first pre-mixed in 50 μl of OPTI-MEM (Invitrogen) to generate transfection complexes (60 min at room temperature), and then added to the cells. After 24 hours, the complexes were removed by replacement with fresh culture medium plus antibiotics. The YFP-based functional assay was performed after further 24 hours.

For patch-clamp experiments, 500,000 HEK-293 cells in 1.5 ml culture medium without antibiotics were mixed with 0.5 ml of OPTIMEM containing 2 μg plasmid DNA and 5 μl Lipofectamine 2000 (previously incubated for 60 min at room temperature to allow formation of lipid/DNA complexes). Cell suspension was then plated as 5–6 drops in the center of 35 mm Petri dishes. After 5–6 hours, each Petri dish received 2 ml of culture medium without antibiotics. After 24 hours, the complexes were removed by replacement with fresh culture medium plus antibiotics. Patch-clamp experiments were carried out 2–3 days after transfection.

2.3. Stable transfections

FRT cells were plated in six-well microplates (300,000 cells/well). After 24 hours, cells were transfected with the plasmids coding for TMEM16A isoforms and Lipofectamine 2000 (2 μg and 5 μl per well, respectively). After 24 hours, cells were selected for 3–4 days with G418 0.75 mg/ml in the culture medium. After this initial phase, cells were detached by trypsinization and seeded in 96-well microplates at a density of approximately one cell per well. Selection in G418 was continued for further 2–3 weeks until individual cell colonies were identified by visual inspection. Cells from each well were trypsinized and further expanded. The clones expressing TMEM16A were identified by protein expression (immunofluorescence) and function (transepithelial Cl^- currents).

2.4. YFP assay

Transfected HEK-293 cells were washed two times with 100 μl PBS (137 mM NaCl, 2.7 mM KCl, 8.1 mM Na_2HPO_4, 1.5 mM KH_2PO_4, 1 mM $CaCl_2$, and 0.5 mM $MgCl_2$; pH = 7.4) and incubated for 30 min with 60 μl PBS. After incubation, cells were transferred to an Olympus IX50 fluorescence microscope equipped with a 20× objective, optical filters for detection of EYFP fluorescence (Chroma; excitation: HQ500/20×, 500 ± 10 nm; emission: HQ535/30M, 535 ± 15 nm; dichroic: 515 nm) and a photomultiplier tube (Hamamatsu). For each well, cell fluorescence was continuously measured before and after addition of 165 μl of a modified PBS containing 137 mM KI instead of NaCl (final I^- concentration in the well: 100 mM) with or without ionomycin 1 μM. The output from the photomultiplier tube was digitized using a PowerLab 2/25 acquisition system (ADInstruments) and stored on a Macintosh computer. After background subtraction, cell fluorescence recordings were normalized for the initial average value measured before addition of I^-. The signal decay caused by YFP fluorescence quenching was fitted with a double exponential function to derive the maximal quenching rate that corresponds to initial influx of I^- into the cells.

2.5. Transepithelial Cl^- current measurements

FRT cells with stable expression of TMEM16A isoforms or null FRT cells were plated on Snapwell inserts 3801 (500,000 cells per insert; Corning Life Sciences). Experiments on FRT cells were performed 3–5 days after plating by mounting the Snapwell inserts in a self-contained Ussing chamber system (vertical diffusion chamber). Transepithelial currents were measured using a transepithelial Cl^- gradient. Accordingly, the basolateral solution contained 130 mM NaCl, whereas the apical solution contained 65 mM NaCl and 65 mM sodium gluconate. The two solutions had also 2.7 mM KCl, 1.5 mM KH_2PO_4, 1 mM $CaCl_2$ (2 mM for apical), 0.5 mM $MgCl_2$, 10 mM Na–HEPES (pH 7.3), and 10 mM glucose. During experiments, solutions in both chambers were continuously bubbled with air. The hemichambers were connected to DVC-1000 voltage clamps (World Precision Instruments, Inc., Sarasota, FL) via Ag/AgCl electrodes and 1 M KCl agar bridges. Transepithelial currents were digitized using PowerLab 4/25 data acquisition systems and stored on a personal computer. All measurements were done at 37 °C.

2.6. Patch-clamp experiments

Whole-cell membrane currents were recorded in HEK-293 and Fischer rat thyroid (FRT) cells after transient and stable transfection, respectively. The extracellular solution in most experiments had the following composition: 150 mM NaCl, 1 mM $CaCl_2$, 1 mM $MgCl_2$, 10 mM glucose, 10 mM mannitol, 10 mM Na-HEPES (pH = 7.4). For ion selectivity experiments, this solution was modified by replacing NaCl with NaI, NaSCN, or sodium gluconate (no additional Ca^{2+} was added to compensate for the Ca^{2+} buffering ability of gluconate). To measure the relative cation/anion permeability, we used two modified extracellular solutions in which NaCl was replaced by 150 mM CsCl (high CsCl) or by 30 mM CsCl plus 230 mM mannitol (low CsCl). The pipette (intracellular) solution contained 130 mM CsCl, 10 mM EGTA, 1 mM $MgCl_2$, 10 mM HEPES, 1 mM ATP (pH = 7.35) plus $CaCl_2$ to obtain the desired free Ca^{2+} concentration: 6 mM for 115 nM, 8 mM for 305 nM, 8.57 mM for 455 nM, 9 mM for 685 nM, 9.27 mM for 965 nM, and 9.5 mM for 1.25 μM (calculated with a dissociation constant for the EGTA–calcium complex of $7.6 \cdot 10^{-8}$ M at pH 7.35). Accordingly, the final Cl^- concentration in the pipette solution ranged from 144 mM to 151 mM in the solutions with the lowest and the highest Ca^{2+} concentration, respectively. During experiments, the membrane capacitance and series resistance were analogically compensated using the circuitry provided by the EPC7 patch-clamp amplifier. The usual protocol for stimulation consisted in 600 ms-long voltage steps from −100 to 100 mV in 20 mV increments starting from a holding potential of −60 mV. The waiting time between steps was 4 s. To measure the reversal potential of TMEM16A(*abc*) currents, we used a different protocol consisting in a preactivating pulse at +80 mV followed by test potentials in the range between −80 and +80 mV. Membrane currents were filtered at 1 kHz and digitized at 5 kHz with an ITC-16 (Instrutech) AD/DA converter. Data were analyzed using the Igor software (WaveMetrics) supplemented by custom software kindly provided by Dr. Oscar Moran.

Liquid junction potentials were calculated with the Patcher's Power Tool (developed by Dr. Francisco Mendes and Franz Wurriehausen, Max Planck Institute for Biophysical Chemistry, Gottingen, Germany) as described previously [11] and used to correct the reversal potential of membrane currents.

The relationship of the conductance vs. the intracellular free Ca^{2+} concentrations for the (*0*) isoform was fitted with a Hill equation:

$$\gamma = \gamma_{max} \Big/ \left(1 + \left(K_d \Big/ \left[Ca^{2+}\right]_i\right)^n\right)$$

where γ is the membrane conductance at a given Ca^{2+} concentration, γ_{max} the maximal conductance value, K_d is the dissociation constant, and n is the Hill coefficient.

For the (*abc*) isoform, given the inactivation caused by high Ca^{2+} concentrations, we used a modified equation:

$$\gamma = \gamma_{max} / \left(1 + \left(K_d / \left[Ca^{2+}\right]_i\right)^n\right) \cdot \left(1 - \left(1 / \left(1 + \left(K_i / \left[Ca^{2+}\right]_i\right)^m\right)\right)\right)$$

where K_i is the inhibitory constant, and m is the coefficient for the inhibitory process.

2.7. Immunofluorescence

FRT and HEK-293 cells were fixed in 25% acetic acid/75% ethanol (vol/vol) for 10 min. After washing in PBS, cells were incubated for 2 hours at room temperature in 1% bovine serum albumin (BSA, Sigma-Aldrich) in PBS. Cells were then incubated overnight at 4 °C with the pre-diluted BV10 primary antibody for TMEM16A (ab66170, Abcam) mixed 1:1 with PBS also containing 0.3% (vol/vol) of Triton X-100 plus 1% BSA. After washing, the cells were incubated with a goat anti-rabbit antibody (1:200 dilution) conjugated with Alexa Fluor 488 (Invitrogen) for 1 hour at room temperature. Images were taken with an Olympus IX50 fluorescence microscope equipped with a 40× objective and a Coolspan camera (Photometrics). All images were acquired with the MetaMorph software using a fixed exposure time and gain.

2.8. Statistics

Data are shown as representative experiments or as mean ± SEM. Statistical significance of differences between groups of data was assessed with the Student's *t* test.

3. Results

3.1. Ion transport ability of TMEM16 protein isoforms

The cartoon in Fig. 1A (top) shows the predicted topology of the TMEM16A protein and the localization of the three alternative segments (*a*), (*b*), and (*c*). Expression of the TMEM16A(*abc*) isoform, carrying the three segments, by transient transfection in HEK-293 cells, caused the appearance of Ca^{2+}-dependent anion transport, as measured with the HS-YFP assay. Indeed, stimulation with the Ca^{2+}-elevating agent ionomycin evoked a strong increase in fluorescence quenching rate reflecting an accelerated I^- influx (Fig. 1B). Expression of TMEM16A(*0*) also caused an increase in Ca^{2+}-dependent I^- transport. Although

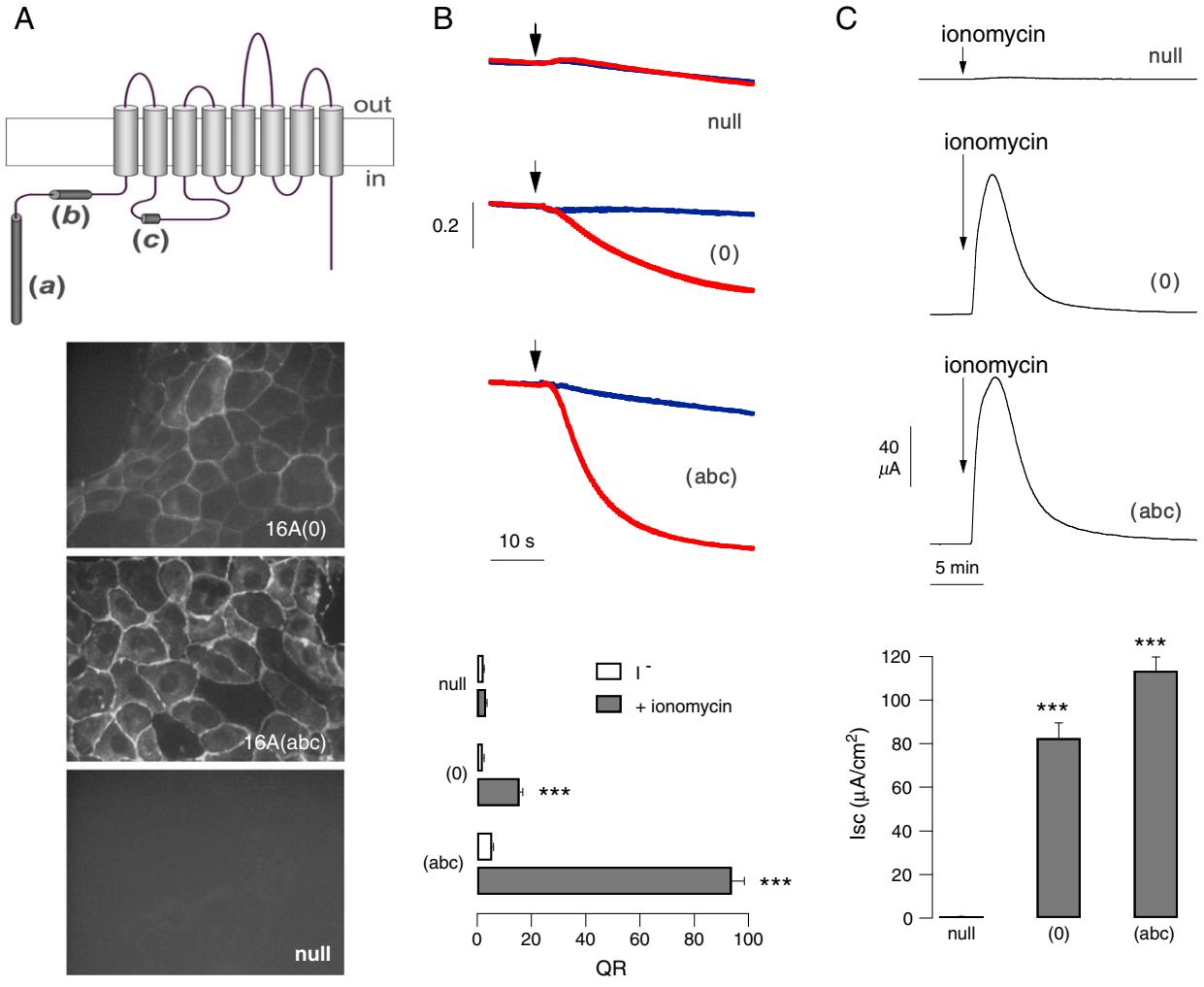

Fig. 1. TMEM16A(*0*) as a membrane protein associated with anion transport activity. A. Topology of TMEM16A with localization of alternative segments *a*, *b*, and *c* (top) and immunofluorescence analysis of 16A(0) and 16A(*abc*) subcellular localization (bottom). Images were taken from stable transfected or from null FRT cells. B. Representative traces (top) and summary of data (bottom) from experiments carried out with the YFP assay on HEK-293 cells transiently transfected with TMEM16A isoforms or empty plasmids. Red and blue traces show the cell fluorescence decrease following I^- addition (arrow) with and without 1 μM ionomycin, respectively. The bar graph reports the maximal quenching rate (QR) by I^-. ***, $p<0.001$ vs. null cells ($n=6$–13). C. Representative traces and statistics from transepithelial Cl^- current experiments. The graph reports the peak current elicited by 1 μM ionomycin. ***, $p<0.001$ vs. null cells ($n=13$–35).

smaller than the transport associated with TMEM16A(*abc*), it was significantly larger than that of mock-transfected cells (Fig. 1B).

We also studied TMEM16A(*0*) activity after stable expression in FRT cells and measurement of transepithelial Cl^- currents with the short-circuit current technique (Fig. 1C). Cells expressing TMEM16A (*abc*) and TMEM16A(*0*) responded similarly to ionomycin application with a large and transient increase in Cl^- transport. In contrast, the current elicited by ionomycin in null FRT cells was negligible.

We measured the subcellular localization of TMEM16A isoforms by immunofluorescence. Similarly to TMEM16A(*abc*), the (*0*) isoform showed a pattern consistent with a plasma membrane localization (Fig. 1A). However, the intensity of the immunofluorescence signal was consistently weaker for TMEM16A(*0*).

3.2. Effect of membrane potential

We studied the biophysical properties of TMEM16A(*0*) by patch-clamp recordings in the whole-cell configuration (Figs. 2A, C). At low cytosolic free Ca^{2+} concentrations (≤115 nM), TMEM16A(*0*)-expressing FRT cells showed very small currents, not different from those of null cells. However, the membrane currents became progressively larger as the cytosolic Ca^{2+} was increased from 115 to 685 nM. Interestingly, these currents were completely devoid of any relaxation following application of voltage pulses and the shape of the corresponding current–voltage relationship was largely linear (Figs. 2A, C). Cells expressing TMEM16A(*abc*) also showed membrane currents dependent on Ca^{2+} concentration (Figs. 2B, D). However, these currents were markedly voltage-dependent, with a strong activation at positive membrane potentials, as shown previously [11,19]. The resulting current–voltage relationship was characterized by outward rectification (Fig. 2D).

To quantify the Ca^{2+}-dependence of the channels associated with the (*0*) and (*abc*) isoforms, we plotted the conductance vs. the intracellular free Ca^{2+} concentration (Fig. 2E). TMEM16A(*0*) data could be fitted with a simple Hill equation giving a K_d of 371 nM for Ca^{2+}. Data for TMEM16A(*abc*) were similar to those obtained for TMEM16A(*0*) in the range between 115 and 965 nM. However, at higher concentrations (e.g. 1.25 μM) the (*abc*)-dependent channels strongly inactivated (Fig. 2E). Interestingly, this phenomenon was absent in cells expressing TMEM16A(*ac*) (not shown). Fitting of TMEM16A(*abc*) data gave a K_d of 387 nM, very close to that of the (*0*) variant, and a K_i of 1.13 μM.

The lack of voltage-dependent activation of TMEM16A(*0*) may be due, at least in part, to the absence of segment (*c*), as shown previously

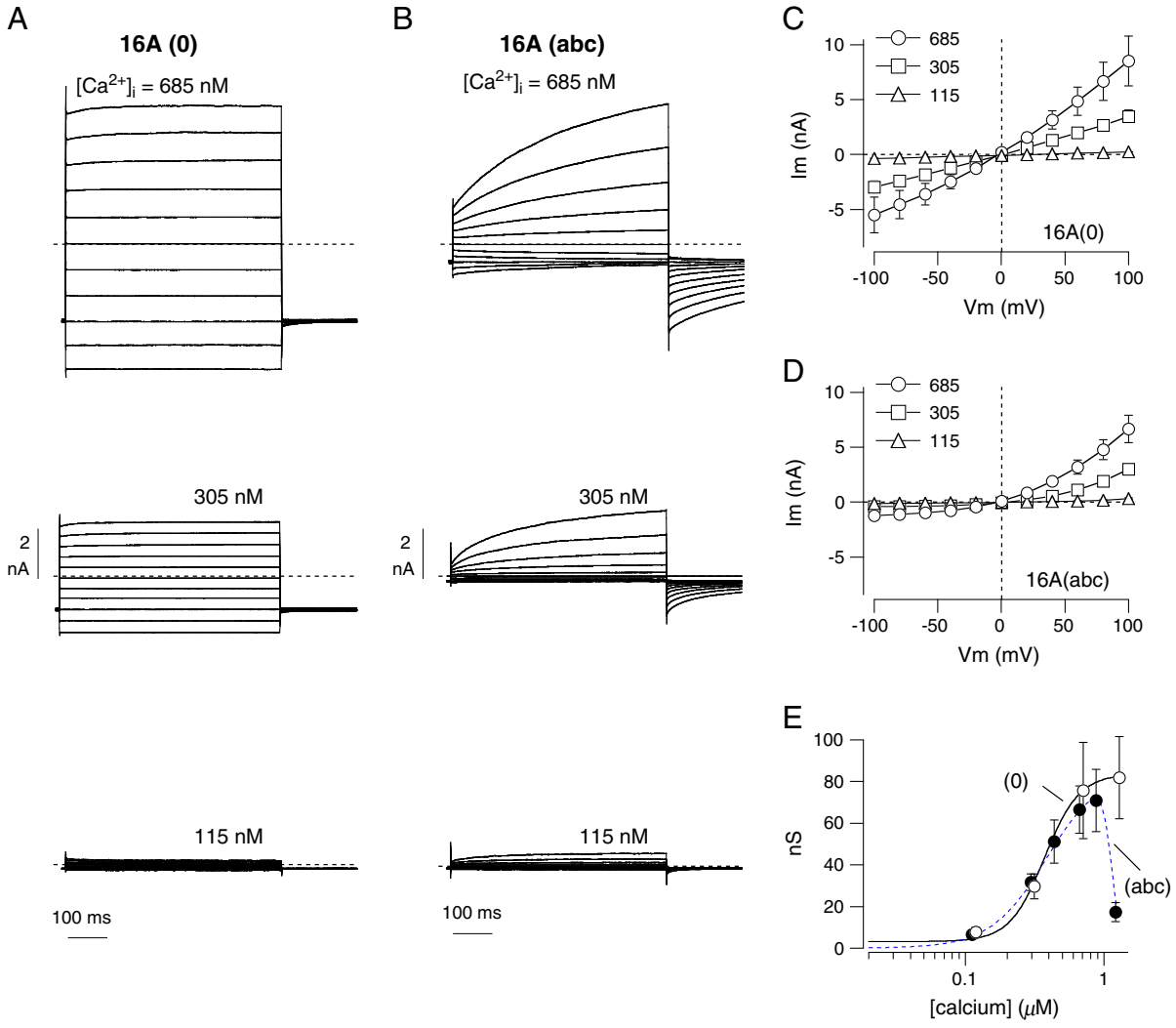

Fig. 2. Properties of membrane currents elicited by TMEM16A isoform expression. A, B. Representative whole-cell membrane currents from patch-clamp experiments on FRT cells with stable expression of TMEM16A(*0*) and TMEM16A(*abc*). Each panel shows superimposed currents elicited at membrane potentials in the range −100 to +100 mV with the indicated free Ca^{2+} concentration in the pipette solution. C, D. Corresponding current–voltage relationships from similar experiments (n = 7–48). The amplitude of the currents was taken as the maximal level reached at the end of the test pulse. E. Plot of the maximal conductance elicited at +100 mV vs. the cytosolic free Ca^{2+} concentration for the (*0*) and the (*abc*) variants. Data are fitted as described in Materials and methods.

[19]. However, we asked whether the absence of the 116 amino acids corresponding to segment *a* has also an effect on the voltage-dependence of the channel. Therefore, we transfected HEK-293 cells with a plasmid coding for a mutated form of TMEM16A(*abcd*) in which the first ATG in the coding sequence is replaced with a stop codon. In this way, the translation is forced to start at the subsequent methionine localized immediately after segment *a*. Expression of this protein, termed TMEM16A(*bcd*) and lacking the first 116 amino acids, resulted in currents having voltage-dependent activation at positive membrane potentials similarly to the full protein (Fig. 3).

3.3. Ion selectivity of TMEM16A channels

We asked whether TMEM16A(*0*)-dependent channels are anion-selective. Therefore, during whole-cell patch-clamp recordings, we lowered extracellular Cl^- concentration or replaced Cl^- with gluconate, I^-, or SCN^-. To elicit channel activity, we used the pipette solution with a free Ca^{2+} concentration of 305 nM. To measure changes in the reversal potential of membrane currents following ion substitution, we used two different methods. For TMEM16A(*abc*), which is voltage-dependent, we measured the amplitude of tail currents elicited at different membrane potentials following an activating pulse at +80 mV. In this way, it is possible to measure significant currents at negative membrane potentials, at which the channels are otherwise mostly closed. For TMEM16A(*0*), which is voltage-independent and lacks tail currents, we directly measured the currents elicited by the test pulses at different membrane potentials. Fig. 4A and B shows the results obtained with extracellular gluconate. In cells expressing TMEM16A(*abc*), replacement of extracellular Cl^- with this large anion strongly reduced the outward currents (i.e. Cl^- entering the cells) and shifted the reversal potential to very positive values (from $+11.6 \pm 3.1$ mV with extracellular Cl^-, to $+81.7 \pm 8.0$ mV with extracellular gluconate; $n = 9$). Such results are consistent with a channel highly selective for Cl^-.

In cells expressing TMEM16A(*0*), exposure to extracellular gluconate elicited a more complex response (Fig. 4C, D). First, replacement with gluconate caused a marked decrease in membrane current amplitude at all voltages. For example, the membrane conductance measured at +100 mV decreased from 26.0 ± 5.4 nS to 0.55 ± 0.14 nS ($n = 5$). Under these conditions, the residual currents showed a reversal potential of $+43.6 \pm 5.4$ mV, significantly more positive than the value measured

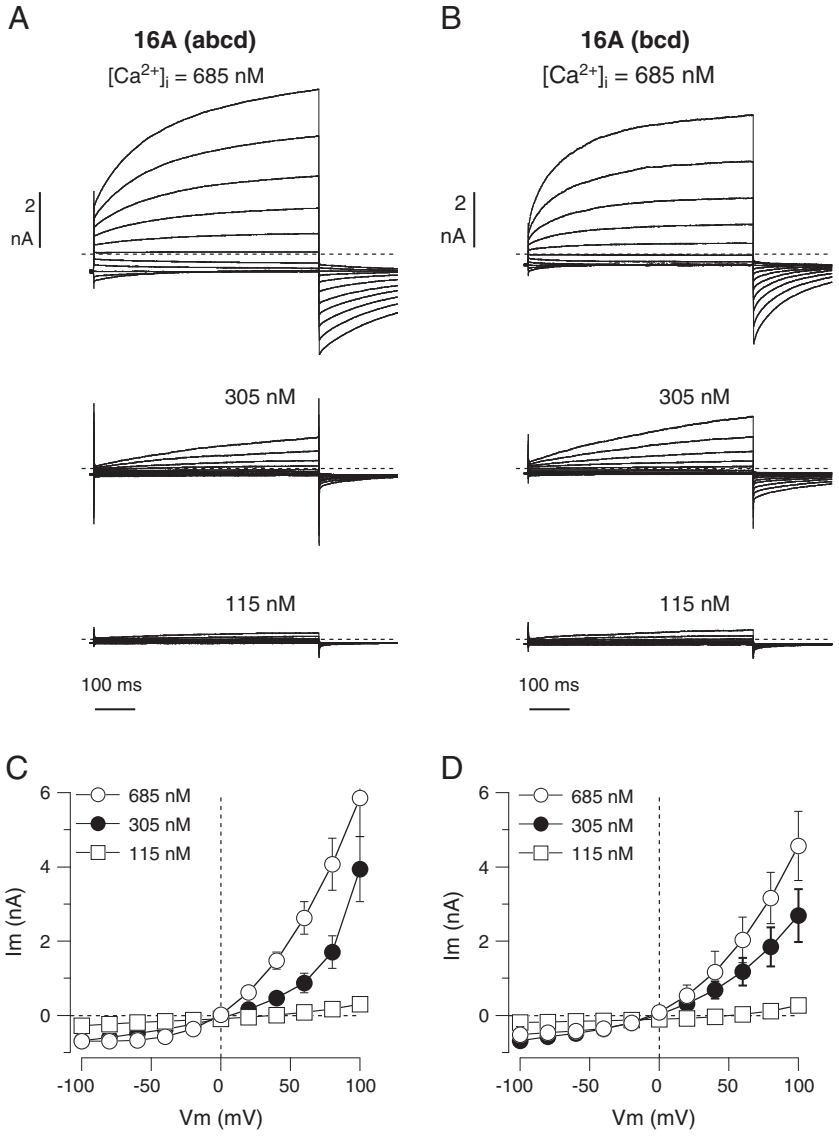

Fig. 3. Membrane currents associated with TMEM16A protein lacking segment *a*. A, B. Representative membrane currents associated with transient transfection of HEK-293 cells with TMEM16A(*abcd*) and TMEM16A(*bcd*). Experiments were carried out at three free Ca^{2+} concentrations in the intracellular solution (115, 305, and 685 nM). C, D. Current–voltage relationships from cells expressing (*abcd*) and (*bcd*) isoforms, respectively.

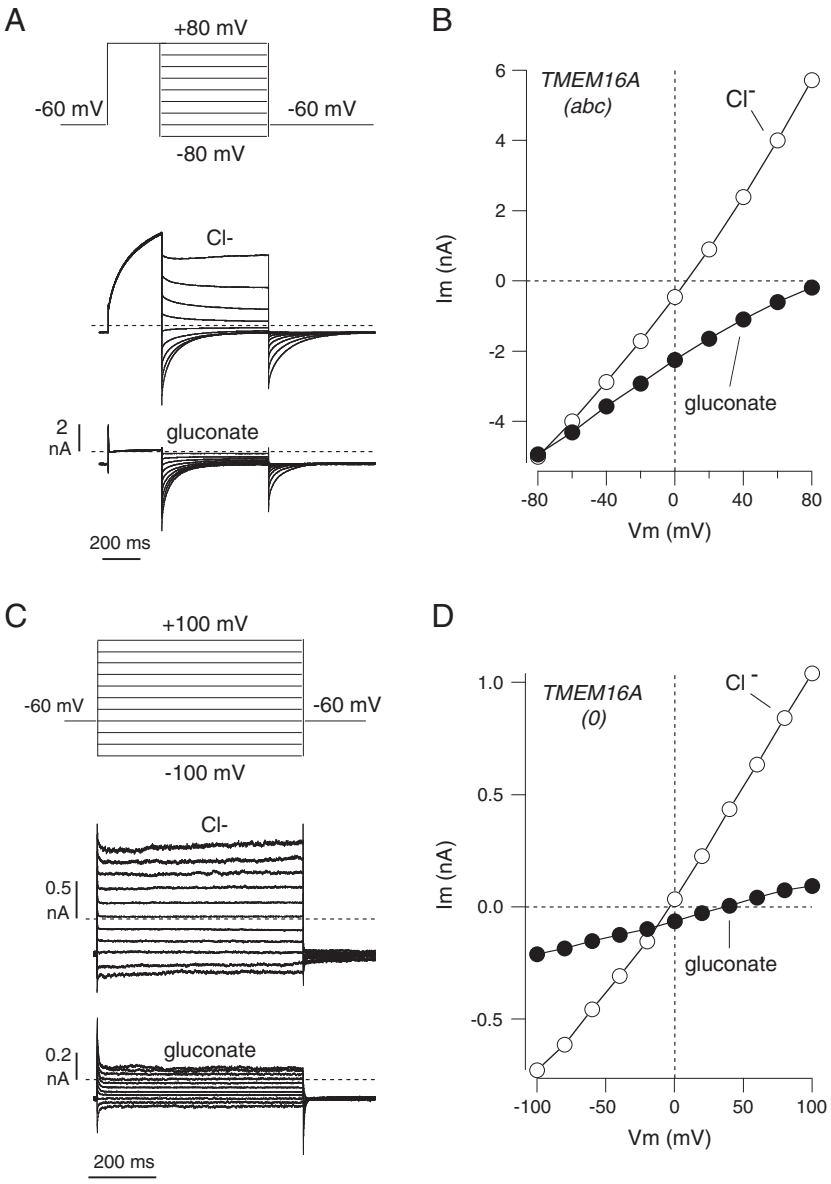

Fig. 4. Effect of extracellular Cl^- replacement with gluconate. A. Scheme of the voltage stimulation protocol and representative traces from an experiment on an FRT cell expressing TMEM16A(*abc*). B. Current–voltage relationship from the same experiment. The graph reports the maximal value of the tail current elicited at different membrane potentials after the pre-activating stimulus at +80 mV. C. Scheme of the voltage stimulation protocol and representative traces from an experiment on an FRT cell expressing TMEM16A(*0*). D. Current–voltage relationship from the same experiment. In these experiments, as well as in those shown in Figs. 5 and 6, the free Ca^{2+} concentration in the pipette solution was 305 nM (total Cl^- concentration: 148 mM).

with high Cl^- before gluconate ($+5.9 \pm 1.2$ mV). It is important to note that inhibition of Cl^- currents by gluconate was not reversible. When gluconate was replaced back with Cl^-, the reversal potential returned to original values but membrane conductance did not recover. Inhibition by gluconate was often observed also for TMEM16A(*abc*) currents but the effect was considerably less dramatic (21.2 ± 3.5 nS with Cl^- and 12.4 ± 2.9 nS with gluconate).

We also evaluated the cation vs. anion permeability of TMEM16A-dependent channels using the high (150 mM) and low (30 mM) CsCl concentrations in the extracellular medium (Fig. 5). For the (*abc*) isoform, lowering of the CsCl concentration shifted the reversal potential of the current from $+5.4 \pm 3.5$ to $+39.1 \pm 5.3$ mV ($n = 4$) (Fig. 5A, B). The latter value is very close to the theoretical Cl^- equilibrium potential (+37 mV). This result indicates that the relative permeability for Cs^+ vs. Cl^- is negligible. For the (*0*) isoform, the lowering of the CsCl concentration had two effects (Fig. 5C, D). First, the reversal potential shifted from $+6.4 \pm 4.4$ to $+29.9 \pm 4.3$ mV ($n = 4$). Therefore, the change in reversal potential is smaller for the (*0*) isoform, thus indicating a detectable permeability to Cs^+ vs. Cl^- ($P_{Cs}/P_{Cl} = 0.09$). The second effect was a decrease (70%) of the conductance at all membrane potentials, similar but much less dramatic than that observed in the presence of gluconate (compare Figs. 4 and 5).

We also measured the permeability to other anions. Fig. 6 shows data obtained by replacing extracellular Cl^- with I^-. FRT cells expressing TMEM16A(*abc*) responded to I^- with a change of the reversal potential to negative values (from $+9.4 \pm 1.9$ mV to -20.5 ± 5.1 mV; $n = 7$) and with a two-fold increase in membrane conductance at all membrane potentials (from 21.2 ± 3.5 nS to 40.2 ± 5.1 nS) (Fig. 6A, B). The reversal potential shift is consistent with a permeability to I^- higher than to Cl^- ($P_I/P_{Cl} = 3.6 \pm 0.7$), as already observed for native CaCCs [21,22]. The increase in membrane conductance by I^- was also reported previously in cells with endogenous expression of CaCCs [21]. In FRT cells expressing TMEM16A(*0*), perfusion with I^- caused a five-fold increase in membrane conductance (26.8 ± 5.4 nS to 131.1 ± 20.5 nS)

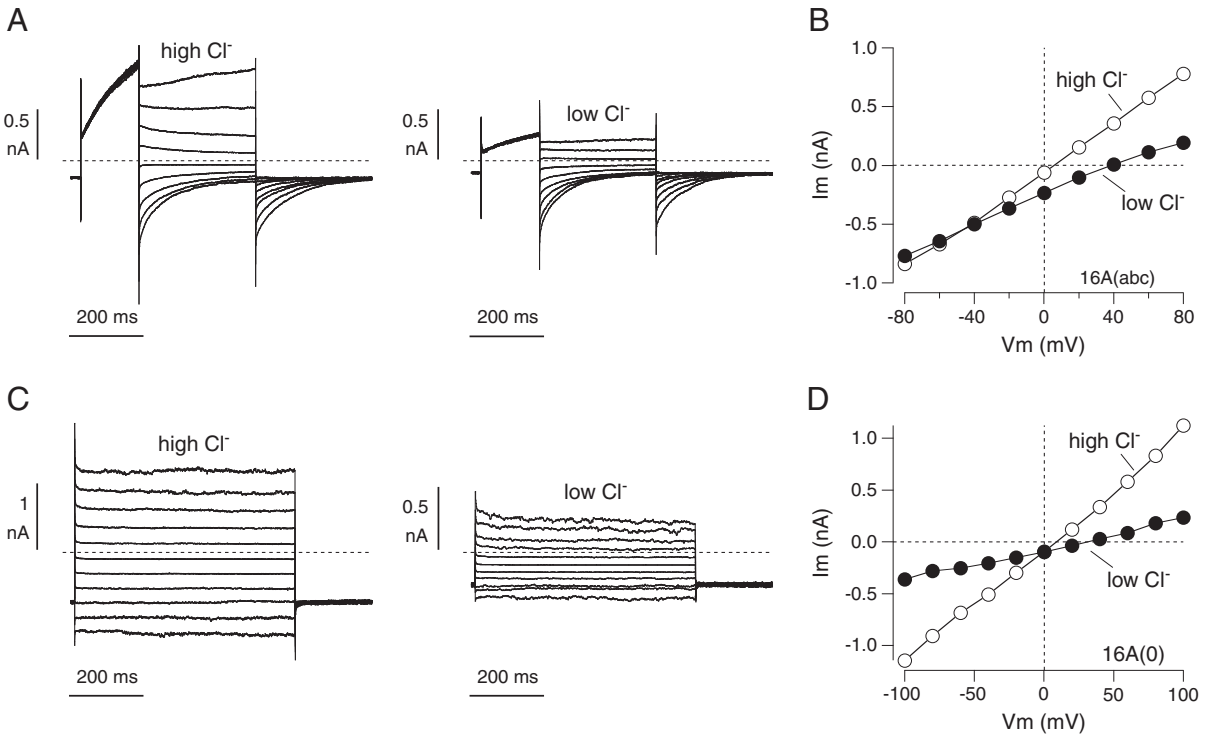

Fig. 5. Determination of the cation/anion relative permeability. A. Tail currents elicited with the protocol depicted in Fig. 4A in an FRT cell expressing the (*abc*) isoform. The traces show the effect of lowering the extracellular CsCl concentration from 150 mM to 30 mM. B. Current–voltage relationship from the same experiment. The graph reports the maximal value of the tail current at each membrane potential. C. Currents measured in an FRT cell expressing the (*0*) isoform with high and low CsCl in the extracellular solution. The voltage stimulation protocol was the same shown in Fig. 4C. D. Current–voltage relationship from the same experiment.

and a negative shift of reversal potential (from $+7.3\pm1.1$ mV with Cl^- to -31.3 ± 2.4 mV with I^-; $n=5$) (Figs. 6C, D). The resulting P_I/P_{Cl} was 4.7 ± 0.5.

We also tested the effect of extracellular SCN^- (not shown). The results were basically similar to those obtained with I^-. SCN^- also increased membrane conductance, particularly for TMEM16A(*0*). The conductance for TMEM16A(*abc*) was 21.2 ± 3.5 nS with Cl^- and 51.6 ± 16.6 nS with SCN^-. The corresponding values for TMEM16A(*0*) were 26.8 ± 5.4 nS and 155.2 ± 5.5 nS, respectively. The reversal potential of TMEM16(*abc*) currents changed from $+8.8\pm1.6$ mV with Cl^- to -21.8 ± 3.1 mV with SCN^- ($n=7$). For TMEM16A(*0*), the values were $+7.7\pm1.3$ mV with Cl^- and -36 ± 2.4 mV with SCN^- ($n=4$). The values of P_{SCN}/P_{Cl} were 3.4 ± 0.3 and 5.6 ± 0.3 for TMEM16A(*abc*) and TMEM16A(*0*), respectively.

3.4. Effect of C-terminus truncations

According to our data, removal of the first 116 amino acids of the TMEM16A protein does not grossly alter the associated CaCC activity. We wondered about possible effects generated by truncation of the carboxi-terminus. By mutagenesis, the carboxi-terminus of TMEM16A (*abc*) was shortened by 6 (Y977X), 30 (E953X), 45 (Q938X), and 136 (D847X) amino acids (Fig. 7A). The last mutation is localized before the last transmembrane domain. Using the HS-YFP assay on transiently transfected HEK-293 cells, we found that all mutants had activity comparable to that of the wild type protein, with the exception of D847X, which was totally inactive (Fig. 7B). We studied by patch-clamp technique the properties of Q938X, the active mutant with the largest carboxy-terminal deletion. This mutant was associated with voltage-dependent currents similar to those of the wild type protein (Fig. 7C). By immunofluorescence, we looked at the subcellular localization of wild type and mutant TMEM16A protein (Fig. 7D). In HEK-293 cells transiently transfected with TMEM16A (*abc*), we found a pattern consistent with expression of the protein in the plasma membrane. A similar result was also obtained for the Q938X mutant, although an intracellular localization was also observed in some cells. In contrast, the D847X protein was observed only in the perinuclear region (Fig. 7D).

4. Discussion

The study of TMEM16A isoforms, having different combinations of alternative segments, appears very important to identify the domains of the protein involved in channel function and its regulation [19]. We previously identified an isoform, termed TMEM16A(*0*), which is devoid of all alternative segments [11]. Transient transfection of TMEM16A(*0*) generated currents quite different from those associated with other isoforms. In particular, TMEM16A(*0*)-dependent currents lacked the typical activation by membrane depolarization. However, it remained to be determined whether TMEM16A(*0*) channels are also anion-selective and regulated by Ca^{2+}. It has been also considered that TMEM16A(*0*) may be a non-functional isoform of the TMEM16A protein [23]. Although TMEM16A(*0*) seems to have in general a low expression [19], it may be specifically present in some highly specialized cell types. For example, CaCCs devoid of voltage-dependence have been observed in olfactory sensory neurons [8,9] and in renal epithelial cells [24].

In the present study, we report evidence that TMEM16A(*0*) expression is indeed associated with Cl^- channel activity. First, transient and stable expression of TMEM16A(*0*) in HEK-293 and FRT cells, respectively, causes the appearance of Ca^{2+}-dependent ion transport, as measured by three different functional assays. In particular, patch-clamp experiments on stable-transfected cells confirm that the activity of TMEM16A(*0*)-dependent channels is voltage-independent. Second, TMEM16A(*0*) channels are regulated by cytosolic Ca^{2+}. Under resting conditions the channels are closed but rapidly activate following a cytosolic Ca^{2+} increase (HS-YFP and short-circuit current assays). In patch-clamp experiments, the amplitude of the membrane currents in TMEM16A(*0*)-expressing cells is positively correlated with cytosolic

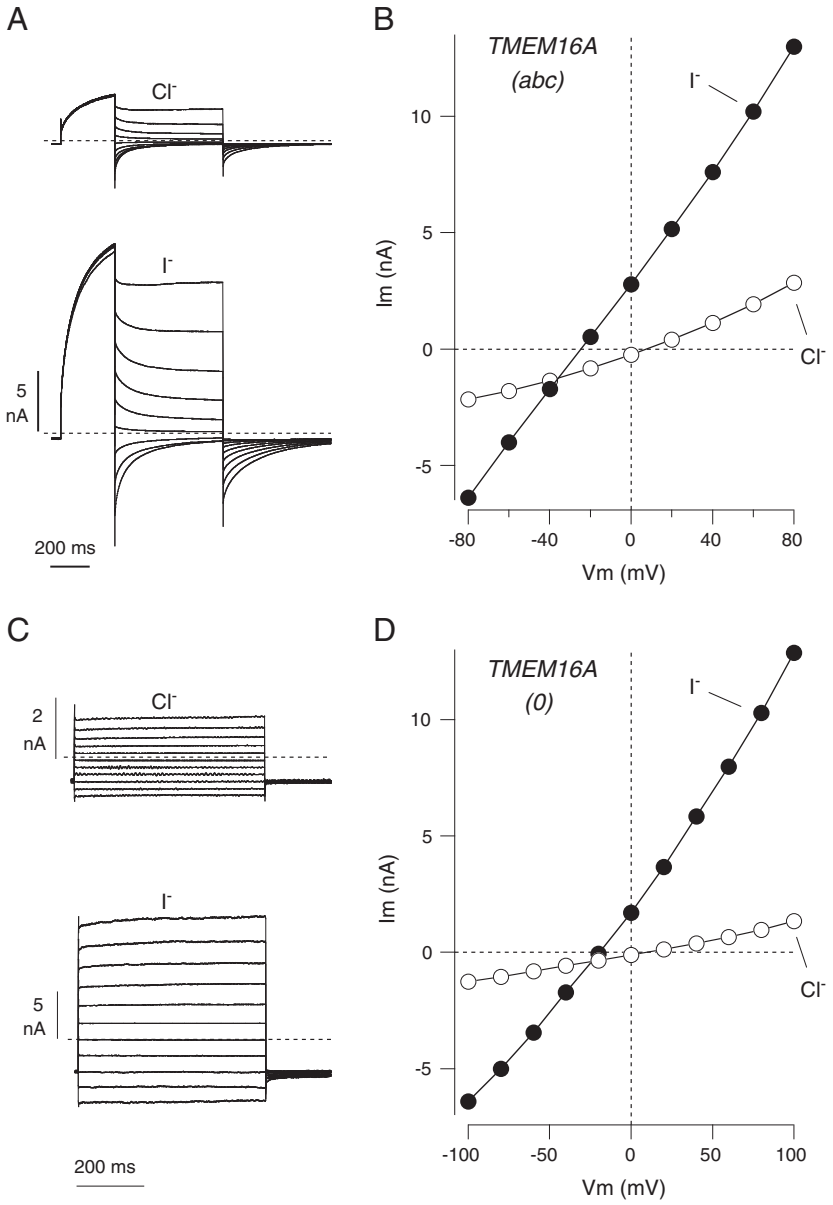

Fig. 6. Effect of extracellular Cl^- replacement with I^-. A–D. Representative experiments (traces and current–voltage relationships) obtained from FRT cells expressing TMEM16A (*abc*) (A, B) or TMEM16A(*0*) (C, D). The voltage protocols were the same as those shown in Fig. 4A and C, respectively.

free Ca^{2+} concentration. The apparent Ca^{2+} affinity controlling channel activation appears similar between the (*0*) and the (*abc*) isoforms. Third, TMEM16A(*0*) channels are anion-permeable. In particular, the permeability to SCN^- and I^- is higher than that to Cl^-, as also observed for TMEM16A(*abc*) and native CaCCs [1,12,13,21,22].

When comparing functional data with protein expression, we found that immunofluorescence detection of TMEM16A(*0*) gave a weaker signal compared to TMEM16A(*abc*), despite comparable levels of ion transport. This could occur if the antibody used in our study is less efficient in detecting the TMEM16A(*0*) protein. Alternatively, TMEM16A(*0*) could be indeed expressed at lower levels but has a higher intrinsic ion transport ability.

It is important to note that, despite the similarities, the channels associated with TMEM16A(*0*) expression appeared less selective for Cl^- versus gluconate when compared to TMEM16A(*abc*). After replacement of extracellular Cl^- with gluconate, the reversal potential of TMEM16A(*0*) currents was significantly less positive than the value obtained with TMEM16A(*abc*). However, we need to consider that the strong inhibition of TMEM16A(*0*) currents by gluconate may have caused an underestimation of selectivity to Cl^-. This inhibition by gluconate, also observed to a lower extent for TMEM16A(*abc*), does not appear to be due to a direct block of channel pore since it cannot be reversed by gluconate washout.

To further investigate the ion selectivity of the two TMEM16A isoforms, we measured the reversal potential of membrane currents at two extracellular CsCl concentrations. These experiments confirmed the impression that the (*0*) isoform has an altered selectivity when compared to TMEM16A(*abc*). Indeed, TMEM16A(*0*) has a measurable permeability to Cs^+ relative to Cl^-.

Another significant observation in our experiments was the membrane conductance increase observed when extracellular Cl^- was replaced with I^- or SCN^-. This effect, already reported for native CaCCs [21], occurred at all voltages. Therefore, it is not simply due to a change in the driving force (which is expected at positive membrane potentials) but also to an increase in single channel conductance and/or open channel probability. Interestingly, the membrane conductance

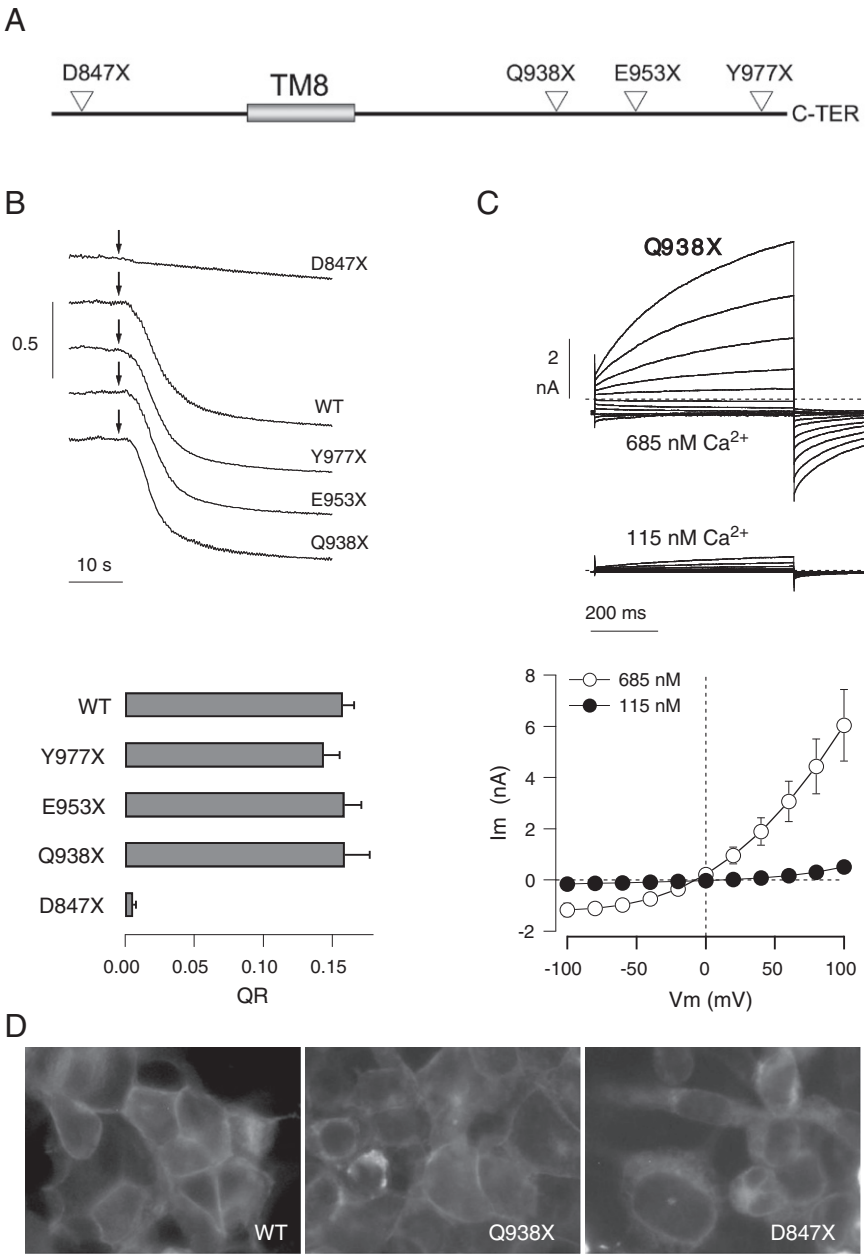

Fig. 7. Truncations of the TMEM16A carboxi-terminus. A. Localization of the non-sense mutations introduced in the TMEM16A(*abc*) coding sequence to generate truncations of the corresponding protein. TM8: transmembrane domain 8. B. Representative traces (top) and statistics (bottom) from experiments done on transiently-transfected HEK-293 cells with the YFP assay. Arrows indicate the addition of extracellular I^- solution plus ionomycin (1 μM). The bar graph reports the quenching rate for wild type and mutant TMEM16A ($n=4$–5). The D847X mutant showed a consistently lower I^- transport rate. C. Whole-cell patch-clamp data (representative membrane currents and average current–voltage relationships) from HEK-293 cells transiently transfected with the Q938X mutant. The free Ca^{2+} concentration in the pipette solution was 685 nM ($n=9$) or 115 nM ($n=8$). D. Immunofluorescence analysis of wild type and mutant TMEM16A protein expression in transiently transfected HEK-293 cells.

increase by I^- and SCN^- was larger for TMEM16A(*0*) than for TMEM16A(*abc*) (~2-fold vs. ~6-fold, respectively).

To summarize, our results suggest that the TMEM16A(*0*) protein represents a basic version of the Ca^{2+}-activated Cl^- channel, having the pore and, at least, part of the Ca^{2+} sensors. The inclusion of additional domains, such as segment (*b*) and segment (*c*), may add other features like voltage-dependent control of channel gating and modulation of ion selectivity/conductance. The possible modification of channel pore properties by regions of the protein that are not expected to be localized within the plasma membrane may be due to allosteric effects. In this regard, it has been reported that TMEM16A-dependent channels have variable ion selectivity due to the possible existence of multiple channel states [12]. A similar observation has been also reported for TMEM16B channels [25].

In our study, we have also begun to investigate the role of the TMEM16A carboxi-terminus. We have found that truncations of the protein cytosolic tail, downstream the last transmembrane segment, do not grossly alter channel activity. However, we cannot exclude that the terminal part of TMEM16A is required for other processes such as interaction with scaffolding and regulatory proteins.

While comparing the Ca^{2+}-dependence of (*0*) and (*abc*) variants, we found that the latter type of TMEM16A protein generates Cl^- currents

which strongly inactivate at very high Ca^{2+} concentrations. This phenomenon, which may have an important physiological role, requires further investigation.

In conclusion, TMEM16A(*0*) may represent a useful backbone, suitable for structure–activity relationship studies in which progressive additions of alternative segment regions will help in elucidating their functional roles.

Acknowledgments

This work was supported by funds from Cystic Fibrosis Foundation, Telethon Foundation [GGP10026], and Fondazione Italiana Fibrosi Cistica [FFC#2/2009] with the contribution of "Delegazione FFC di Vicenza."

References

[1] C. Hartzell, I. Putzier, J. Arreola, Calcium-activated chloride channels, Annu. Rev. Physiol. 67 (2005) 719–758.
[2] J.E. Angermann, A.R. Sanguinetti, J.L. Kenyon, N. Leblanc, I.A. Greenwood, Mechanism of the inhibition of Ca^{2+}-activated Cl^- currents by phosphorylation in pulmonary arterial smooth muscle cells, J. Gen. Physiol. 128 (2006) 73–87.
[3] J. Arreola, J.E. Melvin, T. Begenisich, Activation of calcium-dependent chloride channels in rat parotid acinar cells, J. Gen. Physiol. 108 (1996) 35–47.
[4] S.H. Boese, O. Aziz, N.L. Simmons, M.A. Gray, Kinetics and regulation of a Ca^{2+}-activated Cl^- conductance in mouse renal inner medullary collecting duct cells, Am. J. Physiol. 286 (2004) F682–F692.
[5] I.A. Greenwood, J. Ledoux, N. Leblanc, Differential regulation of Ca^{2+}-activated Cl^- currents in rabbit arterial and portal vein smooth muscle cells by Ca^{2+}-calmodulin-dependent kinase, J. Physiol. 534 (2001) 395–408.
[6] A. Kuruma, H.C. Hartzell, Bimodal control of Ca^{2+}-activated Cl^- channel by different Ca^{2+} signals, J. Gen. Physiol. 115 (2000) 59–80.
[7] Z. Qu, R.W. Wei, H.C. Hartzell, Characterization of Ca^{2+}-activated Cl^- currents in mouse kidney inner medullary collecting duct cells, Am. J. Physiol. 285 (2003) F326–F335.
[8] M. Hallani, J.W. Lynch, P.H. Barry, Characterization of calcium-activated chloride channels in patches excised from the dendritic knob of mammalian olfactory receptor neurons, J. Membr. Biol. 161 (1998) 163–171.
[9] S.J. Kleene, R.C. Gesteland, Calcium-activated chloride conductance in frog olfactory cilia, J. Neurosci. 11 (1991) 3624–3629.
[10] W. Xie, M.A. Kaetzel, K.S. Bruzik, J.R. Dedman, S.B. Shears, D.J. Nelson, Inositol 3,4,5,6-tetrakisphosphate inhibits the calmodulin-dependent protein kinase II-activated chloride conductance in T84 colonic epithelial cells, J. Biol. Chem. 271 (1996) 14092–14097.
[11] A. Caputo, E. Caci, L. Ferrera, N. Pedemonte, C. Barsanti, E. Sondo, U. Pfeffer, R. Ravazzolo, O. Zegarra-Moran, L.J.V. Galietta, TMEM16A, a membrane protein associated with calcium-dependent chloride channel activity, Science 322 (2008) 590–594.
[12] B.C. Schroeder, T. Cheng, Y.N. Jan, L.Y. Jan, Expression cloning of TMEM16A as a calcium-activated chloride channel subunit, Cell 134 (2008) 1019–1029.
[13] Y.D. Yang, H. Cho, J.Y. Koo, M.H. Tak, Y. Cho, W.S. Shim, S.P. Park, J. Lee, B. Lee, B.M. Kim, R. Raouf, Y.K. Shin, U. Oh, TMEM16A confers receptor-activated calcium-dependent chloride conductance, Nature 455 (2008) 1210–1215.
[14] S. Pifferi, M. Dibattista, A. Menini, TMEM16B induces chloride currents activated by calcium in mammalian cells, Pflugers Arch. 458 (2009) 1023–1038.
[15] A.B. Stephan, E.Y. Shum, S. Hirsh, K.D. Cygnar, J. Reisert, H. Zhao, ANO2 is the cilial calcium-activated chloride channel that may mediate olfactory amplification, Proc. Natl. Acad. Sci. U.S.A. 106 (2009) 11776–11781.
[16] H. Stöhr, J.B. Heisig, P.M. Benz, S. Schöberl, V.M. Milenkovic, O. Strauss, W.M. Aartsen, J. Wijnholds, B.H. Weber, H.L. Schulz, TMEM16B, a novel protein with calcium-dependent chloride channel activity, associates with a presynaptic protein complex in photoreceptor terminals, J. Neurosci. 29 (2009) 6809–6818.
[17] L.J. Galietta, The TMEM16 protein family: a new class of chloride channels? Biophys. J. 97 (2009) 3047–3053.
[18] J. Suzuki, M. Umeda, P.J. Sims, S. Nagata, Calcium-dependent phospholipid scrambling by TMEM16F, Nature 468 (2010) 834–838.
[19] L. Ferrera, A. Caputo, I. Ubby, E. Bussani, O. Zegarra-Moran, R. Ravazzolo, F. Pagani, L.J. Galietta, Regulation of TMEM16A chloride channel properties by alternative splicing, J. Biol. Chem. 284 (2009) 33360–33368.
[20] L.J. Galietta, P.M. Haggie, A.S. Verkman, Green fluorescent protein-based halide indicators with improved chloride and iodide affinities, FEBS Lett. 499 (2001) 220–224.
[21] P. Perez-Cornejo, J.A. De Santiago, J. Arreola, Permeant anions control gating of calcium-dependent chloride channels, J. Membr. Biol. 198 (2004) 125–133.
[22] Z. Qu, H.C. Hartzell, Anion permeation in Ca^{2+}-activated Cl^- channels, J. Gen. Physiol. 116 (2000) 825–844.
[23] C. Duran, C.H. Thompson, Q. Xiao, H.C. Hartzell, Chloride channels: often enigmatic, rarely predictable, Annu. Rev. Physiol. 72 (2010) 95–121.
[24] J.E. Linley, S.H. Boese, N.L. Simmons, M.A. Gray, A voltage-dependent Ca^{2+} influx pathway regulates the Ca^{2+}-dependent Cl^- conductance of renal IMCD-3 cells, J. Membr. Biol. 230 (2009) 57–68.
[25] C. Sagheddu, A. Boccaccio, M. Dibattista, G. Montani, R. Tirindelli, A. Menini, Calcium concentration jumps reveal dynamic ion selectivity of calcium-activated chloride currents in mouse olfactory sensory neurons and TMEM16b-transfected HEK 293T cells, J. Physiol. 588 (2010) 4189–4204.